Effects of sheared flows on ion-temperature-gradient-driven turbulent transport

Cite as: Physics of Fluids B: Plasma Physics **4**, 319 (1992); https://doi.org/10.1063/1.860280
Submitted: 25 March 1991 . Accepted: 21 October 1991 . Published Online: 04 June 1998

S. Hamaguchi, and W. Horton

Effects of sheared flows on ion-temperature-gradient-driven turbulent transport

S. Hamaguchi
IBM Thomas J. Watson Research Center, Yorktown Heights, New York 10598

W. Horton
Institute for Fusion Studies, The University of Texas at Austin, Austin, Texas 78712

(Received 25 March 1991; accepted 21 October 1991)

Previous studies of the ion-temperature-gradient (ITG) driven turbulence are expanded to include the effect of sheared $\mathbf{E}\times\mathbf{B}$ flows in sheared magnetic fields. The radial eigenmodes are shown to substantially change character by shifting the modes off the rational surface. The new mode structure and growth rate directly affects the transport of both thermal energy and momentum in the sheared flows. The growth rate first increases with small shear flow and then decreases. The theoretical correlation of the shear flow with the thermal transport is important with respect to the transitions observed in tokamaks of a low (L mode) to a high (H mode) thermal confinement state as a function of the poloidal rotation velocity in the shear flow layer. The three-dimensional nonlinear simulations show that the anomalous ion thermal diffusivity is reduced significantly when $dv_E/dx \simeq 2(c_s/L_s)\sqrt{(1+\eta_i)T_i/T_e}$. This condition is thought to be satisfied in a boundary layer in tokamaks with shear flow.

I. INTRODUCTION

Most of the previous theoretical studies of ion-temperature-gradient(ITG) driven turbulent transport considered equilibrium plasma states with no equilibrium plasma flow velocities.[1-4] Theoretical studies[5-7] of drift wave and resistive g stability including the shear flows in the equilibrium have shown that these shear flows can substantially affect the stability of these forms of drift wave turbulence and the associated anomalous transport. A survey of the effect of the shear flow on the stability of various transport modes is given in the recent work of Tajima *et al.*[8] An intrinsic mechanism for the formation of a shear flow boundary layer as a plasma sheath is shown in the studies of Theilhaber and Birdsall.[9] These works reassessing the stability of the transport modes in the presence of shear flow are motivated by the observations of a strong shear flow layer in the edge plasmas of tokamaks (Ritz *et al.*[10,11] and Taylor *et al.*[12]). Furthermore, the recent transport studies in the large tokamak DIII-D[13,14] showing a sharp increase in the poloidal flow velocity coincident or preceding the change in the thermal confinement properties known as the L- to H-mode transition implicate the shear flow as a contributing factor in the thermal transport of the plasma. Thus it is important to understand the theoretical structure of the well-known ion thermal diffusivity driven by the ion temperature gradient as a function of the sheared perpendicular and parallel ion fluid flow velocities.

In this work we show that the sheared $\mathbf{E}\times\mathbf{B}$ flows directly modify the growth rate and mode widths of the ITG-driven turbulence. As a consequence the mixing length formulas for the ion thermal diffusivities, which have been shown to correlate well with fluxes obtained with full three-dimensional fluid turbulence simulations, are significantly modified by the change in the characteristics of the linear instabilities. The results show that the plasma thermal ion confinement is indeed a function of the state of the equilibrium flows in the system. In this description of the stability and the transport equations obtained from the space-time averages over the small-scale fluctuations in the nonlinear system describe a coupling of the transport of the sheared flow velocity through a Reynolds stress[5,6] and eddy viscosity with the anomalous ion thermal diffusivity.[3] This coupling of the two transport processes makes clear the dependence, in general, of the thermal transport on the equilibrium shear flows.

In these studies we use the fluid model introduced in Hamaguchi and Horton[3,15] which models the effect of ion Landau damping with constant parallel ion viscosity and parallel ion thermal diffusivity of the order of $c_s L_n$. Simple fluid equations such as the ones treated in this paper have the advantage over more complete kinetic equations of being amenable to nonlinear three-dimensional (3-D) simulations. Despite their lack (or less accurate treatment) of some kinetic effects, it is generally acknowledged that appropriate fluid equations give qualitatively correct scalings of various anomalous transport coefficients.[16] We note that Hammet and Perkins[17] have recently developed a more sophisticated model of ion Landau damping in the framework of fluid equations, in which a linear integral operator is constructed for the parallel ion transport terms using a three pole approximation to the Vlasov plasma response function. Discussions on the relationship between kinetic and fluid models are found in Refs. 16 and 17.

The work is organized as follows: In Sec. II the basic nonlinear dynamical equations are given along with the non-dimensional parameters characterizing the equilibrium flows and gradients. In Sec. III the linear stability analysis is present. In Sec. IV, we show results of nonlinear 3-D simulations and calculate the anomalous ion thermal diffusivity in the presence of sheared poloidal flows. Section V contains discussion and conclusions.

 0899-8221/92/020319-10$04.00

II. DYNAMICAL EQUATIONS

The nonlinear evolution equations[3] of the electrostatic ITG-driven mode (or η_i mode) are obtained from the two-fluid equations[18] under the assumptions of charge neutrality ($n_i = n_e = n$), constant electron temperature T_e, zero resistivity, and zero electron inertia. Systematic derivation of the nonlinear evolution equations used in this work is found in Ref. 15. The sheared slab configuration of the magnetic field $\mathbf{B} = B[\hat{\mathbf{z}} + (x - x_0)\hat{\mathbf{y}}/L_s]$ is assumed here, which represents a neighborhood of a rational surface given by $x = x_0$. Here, L_s denotes the shear scale length and $\hat{\mathbf{x}}$, $\hat{\mathbf{y}}$, and $\hat{\mathbf{z}}$ denote the unit vectors of the usual orthogonal coordinate system (x,y,z). In this paper, we do not discuss a toroidal-curvature driven branch of the ITG mode (i.e., the so-called toroidal η_i mode).[19,20] We split each physical quantity into two parts such as $n = n_0(x) + \tilde{n}$; the unperturbed quantity denoted by subscript 0, which is assumed to be a function of only x, and the perturbed quantity denoted by a tilde. It is straightforward to show from the parallel electron momentum balance equation that electrons satisfy a Boltzmann distribution $\tilde{n}/n_0 = e\tilde{\Phi}/T_e$.

For fluctuations localized on a particular rational surface at $x = x_0$, the mean ion flow velocity $\mathbf{v}_{i0}$ may be expanded around the rational surface as

$$\mathbf{v}_{i0}(x) = \mathbf{v}_{i0}(x_0) + (x - x_0)\frac{\partial \mathbf{v}_{i0}}{\partial x} + \cdots.$$

The second term of this expansion may be regarded as a small term compared to the first term $\mathbf{v}_{i0}(x_0)$ in the neighborhood of the rational surface. On the moving frame with the constant velocity $\mathbf{v}_{i0}(x_0)$, therefore, the mean ion flow velocity may be expressed as $\mathbf{v}_{i0} = (x - x_0)\partial \mathbf{v}_{i0}/\partial x$ to the lowest order, which significantly simplifies the system of equations by eliminating terms involving $\mathbf{v}_{i0}(x_0)$. In the present work, we use this moving (inertial) frame to describe the system of equations, in which the magnitude of the mean sheared ion flow $\mathbf{v}_{i0}$ is of the order of the magnitude of ion flow fluctuations $\tilde{\mathbf{v}}_i$. The density-gradient scale length $L_n = -(d \ln n_{i0}/dx)^{-1}$ and the ion temperature gradient scale length $L_T = -(d \ln T_{i0}/dx)^{-1}$ are typical macroscopic scale lengths of the system. In a tokamak, L_n and L_T are generally of the order of the minor radius. The case of a flat-density profile[4] is briefly discussed in Sec. III B.

The appropriate nondimensional space-time variables are

$$\tilde{x} = \frac{x - x_0}{\rho_s}, \quad \tilde{y} = \frac{y}{\rho_s}, \quad \tilde{z} = \frac{z}{L_n}, \quad \tilde{t} = \frac{tc_s}{L_n}$$

and the nondimensional dependent variables are

$$\phi = \frac{e\tilde{\Phi}}{T_e}\frac{L_n}{\rho_s}, \quad v = \frac{\tilde{v}_{\|i}}{c_s}\frac{L_n}{\rho_s}, \quad p = \frac{\tilde{p}_i T_i}{p_{i0} T_e}\frac{L_n}{\rho_s}.$$

With the use of the nondimensional variables, the system of the equations[15] is given by

$$\frac{\partial}{\partial \tilde{t}}(1 - \Delta_\perp)\phi - \{\phi, \Delta_\perp \phi\}$$

$$= -(1 + K\Delta_\perp)\frac{\partial \phi}{\partial \tilde{y}} - S_\perp \tilde{x}(1 - \Delta_\perp)\frac{\partial \phi}{\partial \tilde{y}}$$

$$- S_\perp \frac{\partial^2 p}{\partial \tilde{x}\,\partial \tilde{y}} - \partial_\| v + \{p, \Delta_\perp \phi\} + \left\{\frac{\partial p}{\partial \tilde{x}}, \frac{\partial \phi}{\partial \tilde{x}}\right\}$$

$$+ \left\{\frac{\partial p}{\partial \tilde{y}}, \frac{\partial \phi}{\partial \tilde{y}}\right\} - \mu_\perp \Delta_\perp^2 \phi, \tag{1}$$

$$\frac{\partial v}{\partial \tilde{t}} + \{\phi, v\} = -S_\perp \tilde{x}\frac{\partial v}{\partial \tilde{y}} - S_\| \frac{\partial \phi}{\partial \tilde{y}} - \partial_\|(p + \phi)$$

$$+ \mu_\perp \Delta_\perp v + \mu_\| \partial_\|^2 v, \tag{2}$$

$$\frac{\partial p}{\partial \tilde{t}} + \{\phi, p\} = -S_\perp \tilde{x}\frac{\partial p}{\partial \tilde{y}} - K\frac{\partial \phi}{\partial \tilde{y}} - \Gamma \partial_\| v$$

$$+ \chi_\perp \Delta_\perp p + \chi_\| \partial_\|^2 p, \tag{3}$$

where

$$\tilde{\partial}_\| = s\tilde{x}\frac{\partial}{\partial \tilde{y}} + \frac{\partial}{\partial \tilde{z}},$$

$$\tilde{\nabla}_\perp = \hat{\mathbf{x}}\frac{\partial}{\partial \tilde{x}} + \hat{\mathbf{y}}\frac{\partial}{\partial \tilde{y}}, \quad \tilde{\Delta}_\perp = \nabla_\perp^2,$$

and

$$\{f, g\} = \frac{\partial f}{\partial \tilde{x}}\frac{\partial g}{\partial \tilde{y}} - \frac{\partial f}{\partial \tilde{y}}\frac{\partial g}{\partial \tilde{x}}.$$

The nondimensional parameters used in Eqs. (1)–(3) are given by

$$\eta_i = \frac{L_n}{L_T}, \quad K = \frac{T_i}{T_e}(1 + \eta_i), \quad \Gamma = \frac{\gamma T_i}{T_e}, \quad s = \frac{L_n}{L_s},$$

$$S_\perp = \frac{L_n V_0'}{c_s}, \quad S_\| = \frac{L_n}{c_s}\frac{dv_{\|0}}{dx}.$$

Here, V_0 denotes the y component of the $\mathbf{E}\times\mathbf{B}$ mean flow caused by the mean electric potential Φ_0, where

$$\Phi_0 = (1/2c)(x - x_0)^2 B V_0',$$

with $V_0' = dV_0/dx$ evaluated at $x = x_0$. The constants $\mu_{\perp,\|}$ and $\chi_{\perp,\|}$ in Eqs. (1)–(3) are appropriately chosen dissipation rates. For a collisional plasma the values of $\mu_{\perp,\|}$ and $\chi_{\perp,\|}$ may be taken from the Coulomb transport theory.[18] For the high-temperature tokamak plasmas of interest, the appropriate choice of $\mu_\|$ and $\chi_\|$ is to model the collisionless ion Landau effect.[3] We note that the third term of the right-hand side of Eq. (1), $-S_\perp \partial^2 p/\partial \tilde{x}\,\partial \tilde{y}$, is derived from a so-called nonlinear finite Larmor radius (FLR) term, i.e., $\{\partial p/\partial \tilde{x}, \partial \phi/\partial \tilde{x}\}$ [the sixth term of Eq. (1)] with the substitution of $\phi \to \phi_0 + \phi$, where $\phi_0 \propto \Phi_0 = (x - x_0)^2 B V_0'/2c$.

The domain on which Eqs. (1)–(3) are solved is given by a cubic box $|\tilde{x}| \leqslant L_x$, $0 \leqslant \tilde{y} \leqslant L_y$ and $0 \leqslant \tilde{z} \leqslant L_z$, L_y, and L_z being constants of order unity. The size of the box in the x direction L_x is taken to be large enough, so that when there is magnetic shear ($s \neq 0$), single helicity modes localized at $\tilde{x} = 0$ decay sufficiently as $|\tilde{x}| \to L_x$. In the case of zero shear, $2L_x$ represents the width of a constant background ion-pressure gradient and/or a constant background density gradient. For the boundary conditions of Eqs. (1)–(3), all the dependent variables are assumed to vanish at $|\tilde{x}| = L_x$ and to be periodic in the $\tilde{y}$ and $\tilde{z}$ directions.

We define the space average $\langle\ \rangle$ over the domain by

$$\langle\ \rangle = \frac{1}{2L_x L_y L_z}\int_{-L_x}^{L_x} d\tilde{x}\int_0^{L_y} d\tilde{y}\int_0^{L_z} d\tilde{z}. \tag{4}$$

If L_x is taken to be ∞, the normalization factor $1/2L_x$ needs to be chosen appropriately.[3]

The fluctuation energy balance equation associated with the set of equations (1)–(3) is given by

$$\frac{d}{d\tilde{t}} E_t = S_\perp \left\langle \frac{\partial p}{\partial x}\frac{\partial \phi}{\partial y}\right\rangle - S_\parallel \left\langle v \frac{\partial \phi}{\partial y}\right\rangle - \frac{K}{\Gamma}\left\langle p \frac{\partial \phi}{\partial y}\right\rangle - W_D,$$

where

$$E_t = \tfrac{1}{2}[\langle n^2\rangle + \langle |\nabla_\perp \phi|^2\rangle + \langle v^2\rangle + (1/\Gamma)\langle p^2\rangle]$$

and

$$W_D = \mu_\perp \langle |\Delta_\perp \phi|^2\rangle + \mu_\perp \langle |\nabla_\perp v|^2\rangle + \mu_\parallel \langle |\partial_\parallel v|^2\rangle + \frac{\chi_\perp}{\Gamma}\langle |\nabla_\perp p|^2\rangle + \frac{\chi_\parallel}{\Gamma}\langle |\partial_\parallel p|^2\rangle.$$

The three transport fluxes in the energy balance equations are

$$\left\langle \frac{\partial p}{\partial x}\frac{\partial \phi}{\partial y}\right\rangle \propto \langle \tilde{v}_{dy}\tilde{v}_{Ex}\rangle,$$

$$\left\langle v \frac{\partial \phi}{\partial y}\right\rangle \propto \langle \tilde{v}_\parallel \tilde{v}_{Ex}\rangle,$$

$$\left\langle p \frac{\partial \phi}{\partial y}\right\rangle \propto \langle \tilde{p}_i \tilde{v}_{Ex}\rangle,$$

where $\tilde{v}_{Ex} = -B^{-1}\partial\tilde{\Phi}/\partial y$ and $\tilde{v}_{dy} = (en_iB)^{-1}\partial\tilde{p}_i/\partial x$. These fluxes are proportional to the transverse transports of the y component of the perturbed diamagnetic flow v_{dy}, the perturbed parallel flow $v_{\parallel i}$, and the perturbed ion pressure $\tilde{p}_i$, respectively.

In addition to the fluctuation energy there is kinetic energy in the mean flow field V_0 which is exchanged with the fluctuation energy through the Reynolds stress $\pi = \langle v_{ix}v_{iy}\rangle$. The Reynolds stress gives the change in the mean flow velocity V_0 through the turbulent drag effect in a diffusion time scale as $\partial V_0/\partial t = -\partial\pi/\partial x \simeq \partial_x(\nu_{\text{eddy}}\,\partial V_0/\partial x)$. The Reynolds stress effect is discussed and calculated in Refs. 5 and 6 and thus is not emphasized here.

III. LINEAR STABILITY ANALYSES

A. The eigenmode problem

We now examine linear stability of the ITG-driven mode in the presence of sheared mean flows based on the set of equations (1)–(3). Assuming that the solutions of the linearized equations of the system (1)–(3) have forms such as $\phi = \tilde{\phi}(\tilde{x})\exp i(k\tilde{y} - \tilde{\omega}\tilde{t})$, the complex-valued function $\tilde{\phi}(\tilde{x})$ satisfies

$$s^2\frac{d^2\tilde{\phi}}{dX^2} + \left(\frac{1-\Omega+\Upsilon X}{K+\Omega-\Upsilon X} - k^2 + \frac{X^2(K+B) - XBS_\parallel}{(K+\Omega-\Upsilon X)(AB-\Gamma X^2)}\right)\tilde{\phi} + \frac{\Upsilon s^2}{K+\Omega-\Upsilon X}\frac{d}{dX}\left(\frac{\Gamma X(X-S_\parallel)+AK}{AB-\Gamma X^2}\tilde{\phi}\right) = 0, \tag{5}$$

where X denotes the magnetic-shear scaled radial length defined as $X = sx = L_n(x-x_0)/\rho_s L_s$, $\Upsilon = S_\perp/s = L_s/L_V$ denotes the ratio of the perpendicular flow shear to the magnetic shear with the scale length of the sheared perpendicular flow

$$L_V = L_n/S_\perp = c_s/V_0', \tag{6}$$

k is the normalized wave number in the y direction defined as $k = k_y\rho_s$ and $\Omega = \tilde{\omega}/k = \omega/\omega_e^*$. In Eq. (1)

$$A = \Omega - \Upsilon X + i\mu_\parallel kX^2,$$

$$B = \Omega - \Upsilon X + i\chi_\parallel kX^2.$$

In the absence of parallel (or toroidal) sheared flows ($S_\parallel = 0$), the complex growth rate $\tilde{\omega} = k\Omega$ for a given wave number k is a function of magnetic shear s, the ratio of flow shear to the magnetic shear $\Upsilon = L_s/L_V$ and the ion pressure gradient $K = T_i(1+\eta_i)/T_e$ as well as the (almost fixed) physical parameters Γ, $\mu_\parallel$, and $\chi_\parallel$. It should be noted that the last term of the left-hand side of Eq. (5) comes from the linear second-derivative term of the pressure perturbation in Eq. (1), i.e., $-S_\perp\,\partial^2 p/\partial\tilde{x}\,\partial\tilde{y}$.

In order to analyze effects of the sheared perpendicular flow Υ on the eigenvalue Ω, we begin by setting $\Gamma = S_\parallel = \mu_{\parallel,\perp} = \chi_{\parallel,\perp} = 0$ and $\Upsilon \ll 1$. This is the simplest case where the basic properties of the ITG-driven mode are still maintained and effects of Υ are taken into account as perturbations.

We now expand the eigenvalue Ω and the eigenfunction ϕ in terms of the small quantity Υ, assuming that the mode is localized in such a way that $|X| \sim \mathcal{O}(1)$ (or $|X\Upsilon| \ll 1$). Writing $\Omega = \Omega_0 + \Omega_1 + \Omega_2 + \cdots$ and $\tilde{\phi} = \phi_0 + \phi_1 + \phi_2 + \cdots$, where Ω_1 and ϕ_1 are assumed to be of $\mathcal{O}(|X\Upsilon|)$, and Ω_2 and ϕ_2 are of $\mathcal{O}(|X\Upsilon|^2)$, etc., we obtain as the lowest-order equation

$$s^2\frac{d^2\phi_0}{dX^2} + \left(-k^2 + \frac{1-\Omega_0}{K+\Omega_0} + \frac{X^2}{\Omega_0^2}\right)\phi_0 = 0. \tag{7}$$

In terms of the scaled radial variable ξ,

$$\xi = s^{-1}\alpha^{1/2}X = \alpha^{1/2}x, \tag{8}$$

with

$$\alpha = is/\Omega_0,$$

Eq. (7) may be written as

$$\frac{d^2\phi_0}{d\xi^2} + (E_0 - \xi^2)\phi_0 = 0, \tag{9}$$

where

$$E_0 = (\Omega_0/is)[-k^2 + (1-\Omega_0)/(K+\Omega_0)].$$

The solution of Eqs. (8) and (9) is given by $\phi_0 = \phi_0^{(l)} = e^{-\xi^2/2}H_l(\xi)$ with $E_0 = 2l+1$ or

$$\phi_0 = \phi_0^{(l)}(X) = e^{-iX^2/2s\Omega_0^{(l)}}H_l[(i/2s\Omega_0^{(l)})^{1/2}X], \tag{10}$$

with the eigenvalues Ω_0 satisfying

$$\Omega_0 = \Omega_0^{(l)} = [1/2(1+k^2)]\{1 - k^2K - is(2l+1) \pm \sqrt{[1-k^2K-is(2l+1)]^2 - 4is(2l+1)(1+k^2)K}\}. \tag{11}$$

Here, $H_l(\xi)$ denotes the l th-order Hermitian function of the complex variable ξ. For a long-wavelength mode, which is not the fastest growing mode, the eigenvalue (9) is simplified to

$$\Omega_0^{(l)} \simeq i(2l+1)sK \tag{12}$$

under the assumption that $(2l+1)s \ll 1$ and $|k^2K| \ll 1$. The mode satisfying $k^2 \simeq K^{-1}$ is known to have the largest growth rate,[3] which is derived from Eq. (9) as

$$\Omega_0^{(l)} \simeq (-1+i)(K/2)\sqrt{2(2l+1)s/(K+1)} \tag{13}$$

under the assumption that $|1-k^2K| \lesssim (2l+1)s \ll 1$. The most unstable mode is found by maximizing the normalized growth rate $\tilde{\gamma}_G = k\Omega_0$ with respect to the y-direction wave number $k = k_y\rho_s$ and the radial-mode number l. More details of the solution of Eq. (7) are found in Ref. 3, including the threshold calculations for $K_{\rm crit} = (1+\eta_{i,\rm crit})T_i/T_e$.

Proceeding to the first-order equation of the small Υ expansion, we have

$$\frac{d_2\phi_1}{d\xi^2} + (E_0 - \xi^2)\phi_1 + i\frac{\Omega_0}{s}\frac{K+1}{(K+\Omega_0)^2}(\Omega_1 - \xi\delta)\phi_0 + 2\xi^2\left(\frac{\Omega_1 - \xi\delta}{\Omega_0}\right)\phi_0 + \frac{K\delta}{(K+\Omega_0)\Omega_0}\frac{d}{d\xi}\phi_0 = 0, \tag{14}$$

where

$$\delta = s\Upsilon\alpha^{-1/2} = (-is\Omega_0)^{1/2}\Upsilon,$$

$E_0 = 2l+1$, $\Omega_0 = \Omega_0^{(l)}$, and $\phi_0 = \phi_0^{(l)} = e^{-\xi^2/2}H_l(\xi)$. The solvability condition for the inhomogeneous equation is given by integration of the product of $\phi_0^{(l)}$ and the left-hand side of Eq. (14) over the total domain of ξ; i.e., $-\infty < \xi < \infty$. Since $\phi_0^{(l)}$ is even (odd) if l is even (odd), the solvability condition yields

$$\Omega_1\left(i\frac{\Omega_0}{s}\frac{K+1}{(K+\Omega_0)^2}\langle\phi_0^2\rangle + 2\frac{1}{\Omega_0}\langle\xi^2\phi_0\rangle\right) = 0$$

or, simply,

$$\Omega_1 = 0, \tag{15}$$

where $\langle\ \rangle$ enclosing a function of ξ denotes an integration over the total domain of ξ, i.e.,

$$\langle f\rangle = \int_{-\infty}^{\infty} f(\xi)d\xi. \tag{16}$$

The first-order solution $\phi_1 = \phi_1^{(l)}(\xi)$ may also be calculated from Eq. (14). Expanding $\phi_1^{(l)}$ in terms of the complete orthogonal system $\{\phi_0^{(m)}(\xi)\}$ given in Eq. (9) as

$$\phi_1^{(l)}(\xi) = \sum_{m\neq l} a_m\phi_0^{(m)}(\xi) \tag{17}$$

and substituting this form into Eq. (14) yields

$$\frac{d^2\phi_1}{d\xi^2} + (E_0 - \xi^2)\phi_1 = \sum_{m\neq l} a_m[(2l+1) - (2n+1)]\phi_0^{(m)} = i\frac{\Omega_0}{s}\frac{(K+1)\delta}{(K+\Omega_0)^2}\xi\phi_0^{(l)} + \frac{2\delta}{\Omega_0}\xi^3\phi_0^{(l)} - \frac{K\delta}{(K+\Omega_0)\Omega_0}\frac{d\phi_0^{(l)}}{d\xi}. \tag{18}$$

For the sake of simplicity, we only consider the case of $l = 0$, in which only a_1 and a_3 take nonzero values, as shown in the following. Multiplying Eq. (17) by $\phi_0^{(1)}$ and integrating the resulting equation over $-\infty < \xi < \infty$, we obtain

$$a_1 = -\frac{\delta}{4}\left(i\frac{\Omega_0}{s}\frac{(K+1)}{(K+\Omega_0)^2} + \frac{3}{\Omega_0} + \frac{K}{(K+\Omega_0)\Omega_0}\right). \tag{19}$$

Similarly, by multiplying Eq. (17) by $\phi_0^{(3)}$ and integrating the resulting equation over $-\infty < \xi < \infty$, we obtain

$$a_3 = -\delta/24\Omega_0. \tag{20}$$

In deriving Eqs. (19) and (20), we have used the integral formulas of the zeroth-order eigenfunctions $\phi_0^{(l)}$ summarized in the Appendix.

We thus obtained the perturbed eigenfunction given by

$$\phi(\xi) = \phi_0^{(0)}(\xi) + a_1\phi_0^{(1)}(\xi) + a_3\phi_0^{(3)}(\xi),$$

where $\phi_0^{(1)}(\xi) = 2e^{-\xi^2/2}\xi$ and $\phi_0^{(3)} = 4e^{-\xi^2/2}(2\xi^3 - 3\xi)$. The opposite-parity eigenfunctions $\phi_0^{(1)}$ and $\phi_0^{(3)}$, which are added to the "pure" η_i mode $\phi_0^{(0)}$ as perturbation, represent a shift of the mode off the rational surface. In the case of long-wavelength modes ($|k^2K| \ll 1$) in weak magnetic shear [$(2l+1)s \ll 1$], we use the expression (12) for $\Omega_0^{(0)}$ and simplify a_1 and a_2 as

$$a_1 = (i/\sqrt{K})\Upsilon, \quad a_3 = (i/24\sqrt{K})\Upsilon \tag{21}$$

by using $\delta = (-is\Omega_0)^{1/2}\Upsilon = s\sqrt{K}\,\Upsilon$ and taking the lowest order of a_1 and a_3 in s. Therefore, the eigenfunction in the presence of small poloidal shear flow may be expressed as

$$\tilde{\phi}(x) = e^{-x^2/2K}[1 + (3i\Upsilon/2K)x(1 + 2x^2/9K)]. \tag{22}$$

Since the first-order eigenvalue Ω_1 is 0, we need to proceed to the next order in order to obtain the lowest-order effect of the shear flow Υ on the growth rate. Using $\Omega_1 = 0$, the second-order equation is given by

$$\frac{d^2\phi_2}{d\xi^2} + [(2l+1) - \xi^2]\phi_2 - i\frac{\Omega_0}{s}\frac{(K+1)\delta}{(K+\Omega_0)^2}\xi\phi_1 - 2\frac{\delta\xi^3}{\Omega_0}\phi_1 + \frac{i\Omega_0\Omega_2(K+1)}{s(K+\Omega_0)^2}\phi_0 + \left(\frac{2\Omega_2}{\Omega_0} - \frac{i\Omega_0}{s}\frac{(K+1)}{(K+\Omega_0)^3}\delta^2\right)\xi^2\phi_0 - \frac{3\delta^2}{\Omega_0^2}\xi^4\phi_0 + \frac{K\delta^2}{(K+\Omega_0)\Omega_0^2}\phi_0 + \frac{K\delta}{(K+\Omega_0)\Omega_0}\frac{d}{d\xi}\phi_1 + \frac{K(K+2\Omega_0)\delta^2}{(K+\Omega_0)^2\Omega_0^2}\xi\frac{d\phi_0}{d\xi} = 0. \tag{23}$$

In the case of $l=0$, we substitute $\phi_0=\phi_0^{(0)}=e^{-\xi^2/2}$ and $\phi_1=a_1\phi_0^{(1)}+a_3\phi_0^{(3)}$. The solvability condition of Eq. (23) is obtained by multiplying Eq. (23) by $\phi_0^{(0)}$ and integrating the resulting equation over $-\infty<\xi<\infty$ as

$$-\frac{i\Omega_0}{s}\frac{(K+1)}{(K+\Omega_0)^2}\delta\langle\xi\phi_0^{(0)}\phi_1\rangle-\frac{2\delta}{\Omega_0}\langle\xi^3\phi_0^{(0)}\phi_1\rangle+\frac{i\Omega_0}{s}\frac{(K+1)}{(K+\Omega_0)^2}\Omega_2\langle\phi_0^{(0)2}\rangle+\frac{\delta^2K}{(K+\Omega_0)\Omega_0^2}\langle\phi_0^{(0)2}\rangle$$
$$+\left(\frac{2\Omega_2}{\Omega_0}-\frac{i\Omega_0}{s}\frac{(K+1)\delta^2}{(K+\Omega_0)^3}\right)\langle\xi^2\phi_0^{(0)2}\rangle-\frac{3\delta^2}{\Omega_0^2}\langle\xi^4\phi_0^{(0)2}\rangle+\frac{K\delta}{(K+\Omega_0)\Omega_0}\left\langle\phi_0^{(0)}\frac{d}{d\xi}\phi_1\right\rangle$$
$$+\frac{(K+2\Omega_0)\delta^2K}{(K+\Omega_0)^2\Omega_0^2}\left\langle\phi_0^{(0)}\xi\frac{d}{d\xi}\phi_0\right\rangle=0. \tag{24}$$

In the case of long-wavelength modes in weak magnetic shear, Eq. (24) may be further simplified. Using Eq. (12) or $\Omega_0=isK(|\Omega_0|\ll 1)$ and keeping the lowest-order terms of $\mathcal{O}(s^{-2})$, we have

$$-\frac{2\delta}{\Omega_0}\langle\xi^3\phi_0^{(0)}\phi_1\rangle+\frac{\delta^2}{\Omega_0^2}\langle\phi_0^{(0)2}\rangle+\frac{2\Omega_2}{\Omega_0}\langle\xi^2\phi_0^{(0)2}\rangle$$
$$-\frac{3\delta^2}{\Omega_0^2}\langle\xi^4\phi_0^{(0)2}\rangle+\frac{\delta}{\Omega_0}\left\langle\phi_0^{(0)}\frac{d}{d\xi}\phi_1\right\rangle$$
$$+\frac{\delta^2}{\Omega_0^2}\left\langle\phi_0^{(0)}\xi\frac{d}{d\xi}\phi_0\right\rangle=0.$$

It should be noted that ϕ_1 is of $\mathcal{O}(\delta/s)$ and $K\gg|\Omega_0|$. Using the integral formulas in the Appendix, we obtain

$$\Omega_2=3i\delta^2/4sK=\tfrac{3}{4}is\Upsilon^2.$$

Therefore, the second-order accurate eigenvalue $\Omega=\Omega_0+\Omega_2$ is given by

$$\Omega=isK(1+3\Upsilon^2/4K). \tag{25}$$

In terms of dimensional quantities, $\omega=\omega_e^*\Omega$ is given by

$$\omega=i\omega_e^*\left(\frac{L_n}{L_s}\right)\frac{(1+\eta_i)}{T_e/T_i}\left(1+\frac{3(L_s/L_V)^2}{4(1+\eta_i)}\frac{T_e}{T_i}\right). \tag{26}$$

We thus find that the growth rate $\gamma_G=\mathrm{Im}\,\omega$ increases as $\Upsilon^2=(L_s/L_V)^2$ when Υ is small.

We now briefly consider an alternative formulation of the linear equation (5) in which the resulting equation has a structure similar to that in the standard equation for the Kelvin–Helmholtz instability. With the use of

$$f=\phi/(\Omega-X\Upsilon)\ \text{ and }\ g=\Omega-X\Upsilon,$$

it is easy to show that

$$\frac{d^2\phi}{dX^2}=g\frac{d^2f}{dX^2}-2\Upsilon\frac{df}{dX}.$$

Ignoring the effects of parallel compressibility ($\Gamma=0$), parallel shear flow ($S_\parallel=0$) and parallel diffusion ($\mu_\parallel=\chi_\parallel=0$), we may write Eq. (5) as

$$\frac{d}{dX}\left((K+g)g\frac{df}{dX}\right)$$
$$+\left(-k^2+\frac{1-g}{K+g}+\frac{X^2}{g^2}\right)g(K+g)f=0. \tag{27}$$

In order to further simplify this equation, we introduce

$$\zeta=-g/\Upsilon-\alpha\ \text{ with }\ \alpha=K/2\Upsilon$$

and rewrite Eq. (25) as

$$\frac{d}{d\zeta}\left((\zeta^2-\alpha^2)\frac{df}{d\zeta}\right)+\left[-k^2-\frac{\zeta+\alpha+\Upsilon^{-1}}{\zeta-\alpha}\right.$$
$$\left.+\frac{1}{\Upsilon^2}\left(1+\frac{2\Omega}{\Upsilon(\zeta+\alpha)}+\frac{\Omega^2}{\Upsilon^2(\zeta+\alpha)^2}\right)\right]$$
$$\times(\zeta^2-\alpha^2)f=0, \tag{28}$$

where the relation

$$\frac{X^2}{g^2}=\frac{1}{\Upsilon^2}\left(1-\frac{2\Omega}{g}+\frac{\Omega^2}{g^2}\right)$$

is used. In order to obtain an approximate solution of Eq. (28) by means of the Wentzel–Kramers–Brillouin (WKB) method for large ζ, we transform ζ to

$$\eta=(1/2\alpha)\ln|(\zeta-\alpha)/(\zeta+\alpha)|$$

when $\zeta^2-\alpha^2\neq 0$. Noting the relation

$$d\eta=d\zeta/(\zeta^2-\alpha^2),$$

we transform Eq. (28) to

$$\frac{d^2f}{d\eta^2}+p(\zeta)\left(\frac{d\eta}{d\zeta}\right)^2f=0, \tag{29}$$

with

$$p(\zeta)=-k^2+\frac{\zeta+\alpha+\Upsilon^{-1}}{\zeta-\alpha}+\frac{1}{\Upsilon^2}$$
$$\times\left(1+\frac{2\Omega}{\Upsilon(\zeta+\alpha)}+\frac{\Omega^2}{\Upsilon^2(\zeta+\alpha)^2}\right).$$

The WKB solution of Eq. (29) is then given by

$$f\sim\frac{1}{[p(\zeta)]^{1/4}}\exp\left(\pm i\int^\zeta\sqrt{p(\zeta)}d\zeta\right). \tag{30}$$

In general, it is not possible to perform the integration of Eq. (29) analytically for arbitrary Υ and α. However, taking certain limiting cases, such as the strong shear flow limit ($\Upsilon\to\infty$), significantly simplifies Eq. (29). In fact, the solution and the dispersion relation of Eq. (29) in the case of $p(\zeta)=$ const with appropriate boundary conditions are known in simple forms from the theory of the magnetohydrodynamic (MHD) Kelvin–Helmholtz instability.[21] In the context of the present work, however, we proceed to direct numerical calculations of the linearized system, rather than discussing analytical solutions of Eq. (29). Detailed

analyses based on the formulation of Eqs. (28) and (29) will be presented elsewhere in the light of the relation between the ITG mode and the Kelvin–Helmholtz instability. Interested readers are also advised to refer to Refs. 6 and 8, in which the interaction between the drift wave, g modes, and the Kelvin–Helmholtz instability is discussed in some detail both linearly and nonlinearly.

B. Numerical calculations of linear modes

Instead of solving the eigenvalue problem (5), we now solve the linearized system of Eqs. (1)–(3) numerically as an initial-value problem to obtain the most unstable linear modes under various conditions. The linear initial-value code used here is the same as the nonlinear initial-value code used in Sec. III except that all the nonlinear terms in Eqs. (1)–(3) are dropped in the linear code. Details of the numerical code are found in Sec. IV.

Figure 1 shows the dispersion relation of the ITG-driven mode in the presence of perpendicular shear flows. It is shown that the most unstable mode is obtained for $k = k_y\rho_s \simeq 0.7 \sim 0.8$ regardless of the magnitude of shear flow. It is also shown that a large perpendicular sheared flow ($\Upsilon = 2$) has a stabilizing effect on the mode. The parameters used in these calculations are magnetic shear $s = 0.1$, ion pressure gradient $K = (T_i/T_e)(1 + \eta_i) = 3$, and diffusion coefficients $\chi_\parallel = \mu_\parallel = 1, \chi_\perp = \mu_\perp = 0.01$. One of the limitations of the fluid dynamics from the Braginskii equations[18] is the approximation $k_\perp\rho_i \ll 1$ which for the fastest growing mode ($k_y\rho_s \simeq 0.7 \sim 0.8$) in Fig. 1 is not well satisfied. The corresponding local Vlasov calculation leads to a smaller value of γ at $k_\perp\rho_i < 1$ but gives a higher value of γ at $k_\perp\rho_i > 1$ as seen in Fig. 3(b) of Ref. 20.

In Fig. 2, by fixing the y-direction wave number $k = k_y\rho_s = 0.6$, which gives a mode close to the most unstable mode, we show the relation between the growth rate γ_G and the perpendicular-flow shear parameter $\Upsilon = L_s/L_v$ in two different magnetic shear; $s = L_s/L_n = 0.1$ and 0.3. It is seen that the critical value Υ_c of the shear flow parameter Υ for stability is nearly independent of magnetic shear. We also

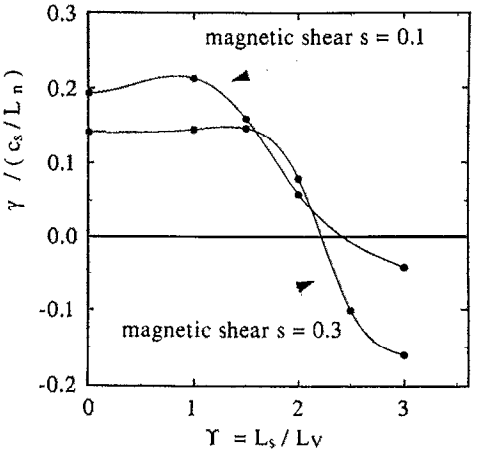

FIG. 2. The relation between the growth rate γ_G and the poloidal flow shear Υ for two different magnetic shear: $s = 0.1$ and 0.3. Here, $K = 3$, $\Gamma = 2$, and $k_y\rho_s = 0.6$.

note that as the perpendicular-flow shear Υ increases from zero, the growth rate γ_G initially increases as a weak function of Υ for small Υ, in accordance with Eq. (25), and then decreases sharply near $\Upsilon = \Upsilon_c$, indicating a transition from the magnetic-shear-dominant region to the flow-shear-dominant region.[22] In the magnetic-shear-dominant region, as shown in many earlier works, the mode structure is sustained and limited by the magnetic shear $s = L_n/L_s$. In the flow-shear-dominant region, the perpendicular-flow shear is so strong that the vortex cells created by the ITG instability are distorted significantly. Figure 3 shows similar relations between γ_G and Υ for two different ion pressure gradients; $K = (T_i/T_e)(1 + \eta_i) = 3$ and 5.

Figure 4 shows the critical value Υ_c of the poloidal flow shear Υ as a function of the ion pressure gradient parameter $K = (1 + \eta_i)(T_i/T_e)$. It is seen that, when K is larger than its critical value K_c ($= 0.4$), Υ_c scales as

$$\Upsilon_c \simeq 2\sqrt{K} = 2\sqrt{(1 + \eta_i)(T_i/T_e)}. \tag{31}$$

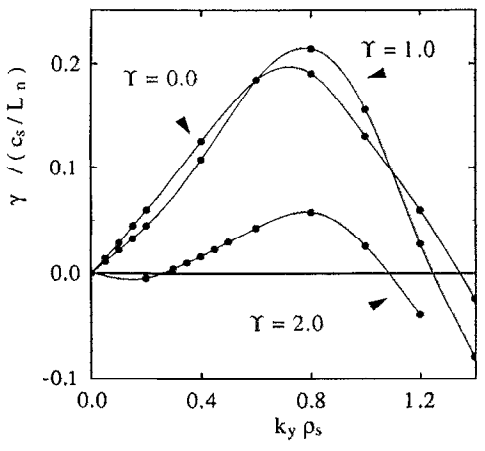

FIG. 1. The dispersion relation of the ITG mode for various Υ values. Here, $K = 3$, $\Gamma = 2$, and $s = 0.1$.

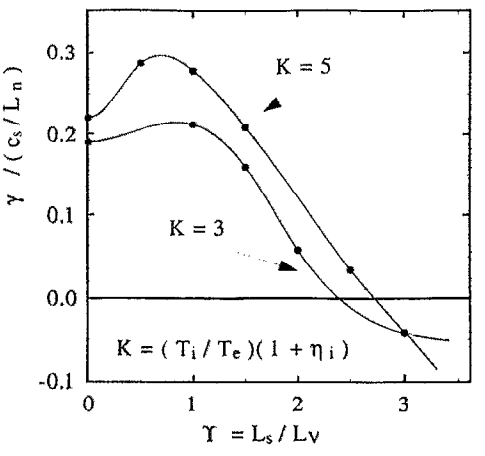

FIG. 3. The relation between the growth rate γ_G and the poloidal flow shear Υ for two different ion temperature gradients: $K = 3$ and 5. Here, $s = 0.1$, $\Gamma = 2$, and $k_y\rho_s = 0.6$.

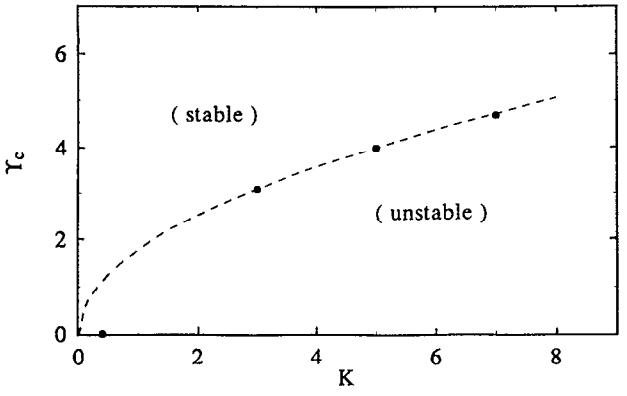

FIG. 4. The critical poloidal flow shear Υ_c as a function of the ion pressure gradient parameter $K=(1+\eta_i)(T_i/T_e)$. The dashed line is a fitting curve given by $\Upsilon_c = 1.78\sqrt{K}$. Note that the critical value for K in the absence of flow ($\Upsilon = 0$) is given by $K_c = 0.4$.

As indicated in Fig. 2, the dependence of Υ_c on magnetic shear s is weak.

We now heuristically derive the formula in Eq. (31). Near the marginally stable state, where $|\Omega| \ll 1$ [Eq. (13) indicates that the real and imaginary parts of the growth rate are of the same order], we may write the eigenmode equation (5) approximately as

$$s^2 \frac{d^2\tilde{\phi}}{dX^2} + \left(\frac{1-\Upsilon X}{K-\Upsilon X} - k^2 + \frac{X^2}{\Omega^2}\right)\tilde{\phi} + \frac{\Upsilon K}{\Omega^2}\frac{d\tilde{\phi}}{dX} = 0, \quad (32)$$

if $\Gamma = \mu_\parallel = \chi_\parallel = 0$ and $K = \mathcal{O}(1)$. Requiring that the sum of the first two terms $(1-\Upsilon X)/(K-\Upsilon X) - k^2$ is of the same order of the third term X^2/Ω^2 in the parentheses ( ) of Eq. (32), we expect $K - \Upsilon X = \mathcal{O}(|\Omega|^2) \ll 1$ near the marginal stable state ($\Upsilon = \Upsilon_c$), where X represents a typical mode width. Equating X to the y-direction mode width of the fastest growing mode given in Eq. (13), namely, $X = k^{-1} \simeq \sqrt{K}$ [or, equivalently $s\Delta x = \Delta y = (k_y\rho_s)^{-1} = \sqrt{K}$, where Δx and Δy are the mode widths normalized by ρ_s], we obtain $K - \Upsilon_c k^{-1} \simeq 0$, i.e., $\Upsilon_c \simeq \sqrt{K}$.

The case of a flat density profile,[4] where $L_n \to \infty$ and $\eta_i \to \infty$, exhibits similar linear properties of the ITG-driven mode to those of the cases of $\eta_i \simeq \mathcal{O}(1)$ presented above. In order to assess the case of a flat density profile, we need to use different normalization of variables and parameters from those used in deriving Eqs. (1)–(3) since the density gradient scale length, which is used as a typical macroscopic scale length, is infinity in this case. An appropriate normalization is given in Ref. 4, where macroscopic lengths are normalized by $(T_e/T_i)L_T$. Under this normalization, Eqs. (1)–(3) with $L_n = \infty$ are transformed to

$$\frac{\partial}{\partial \hat{t}}(1-\Delta_\perp)\hat{\phi} - \{\hat{\phi},\Delta_\perp\hat{\phi}\} = -\Delta_\perp\frac{\partial\hat{\phi}}{\partial\tilde{y}} + \hat{S}_\perp\tilde{x}\Delta_\perp\frac{\partial\hat{\phi}}{\partial\tilde{y}} - \hat{S}_\perp\frac{\partial^2\hat{p}}{\partial\tilde{x}\,\partial\tilde{y}} - \hat{\partial}_\parallel\hat{v} + \{\hat{p},\Delta_\perp\hat{\phi}\} + \left\{\frac{\partial\hat{p}}{\partial\tilde{x}},\frac{\partial\hat{\phi}}{\partial\tilde{x}}\right\} + \left\{\frac{\partial\hat{p}}{\partial\tilde{y}},\frac{\partial\hat{\phi}}{\partial\tilde{y}}\right\} - \hat{\mu}_\perp\Delta_\perp^2\hat{\phi}, \quad (33)$$

$$\frac{\partial\hat{v}}{\partial\hat{t}} + \{\hat{\phi},\hat{v}\} = -\hat{S}_\perp\tilde{x}\frac{\partial\hat{v}}{\partial\tilde{y}} - \hat{S}_\parallel\frac{\partial\hat{\phi}}{\partial\tilde{y}} - \hat{\partial}_\parallel(\hat{p}+\hat{\phi}) + \hat{\mu}_\perp\Delta_\perp\hat{v} + \hat{\mu}_\parallel\hat{\partial}_\parallel^2\hat{v}, \quad (34)$$

$$\frac{\partial\hat{p}}{\partial\hat{t}} + \{\hat{\phi},\hat{p}\} = -\hat{S}_\perp\tilde{x}\frac{\partial\hat{p}}{\partial\tilde{y}} - \frac{\partial\hat{\phi}}{\partial\tilde{y}} - \Gamma\partial_\parallel\hat{v} + \hat{\chi}_\perp\Delta_\perp\hat{p} + \hat{\chi}_\parallel\partial_\parallel^2\hat{p}, \quad (35)$$

where the quantities denoted by the caret have different normalization from those defined in Sec. II, namely,

$$\hat{z} = z/\tau L_T, \quad \hat{t} = tc_s/\tau T_L,$$

$$\hat{\phi} = \frac{e\tilde{\Phi}}{T_e}\frac{\tau L_T}{\rho_s}, \quad \hat{v} = \frac{\tilde{v}_\parallel}{c_s}\frac{\tau L_T}{\rho_s},$$

$$\hat{p} = \frac{\tilde{p}_i}{p_{i0}}\frac{L_T}{\rho_s}, \quad \hat{\partial}_\parallel = \frac{\partial}{\partial\hat{z}} + \sigma\tilde{x}\frac{\partial}{\partial\tilde{y}}$$

and

$$\sigma = \frac{\tau L_T}{L_s}, \quad \tau = \frac{T_e}{T_i}, \quad \hat{S}_\perp = \frac{\tau L_T V_0'}{c_s}, \quad \hat{S}_\parallel = \frac{\tau L_T}{c_s}\frac{dv_{\parallel 0}}{dx}.$$

The diffusion coefficients $\hat{\mu}_\parallel, \hat{\mu}_\perp, \hat{\chi}_\parallel, \hat{\chi}_\perp$ are also normalized accordingly.

We now examine linear properties of the flat density-profile ITG-driven mode with finite shear flow by solving the linearized system of Eqs. (33)–(35) numerically by means of the linear initial-value code.

Figure 5 shows the dispersion relation of the ion-temperature-gradient-driven mode in a flat density profile with $\sigma = \tau L_T/L_s = 0.1$ for four different values of flow shear; $\Upsilon = \hat{S}_\perp/\sigma = L_s/L_V = 0$, 1.0, 1.5, and 1.8. As in Fig. 1, the most unstable mode is obtained for $k_y\rho_s = 0.7 \sim 0.8$. Choosing a wave number $k_y\rho_s = 0.6$, which gives a mode close to the most unstable mode, the relation between the growth rate γ_G and the flow-shear parameter Υ is shown in Fig. 6. As in the cases of finite η_i, the growth rate is an increasing function of Υ for small Υ but decreases steeply near $\Upsilon = \Upsilon_c \simeq 2$. It is evident in Fig. 6 that, for a wide range of the

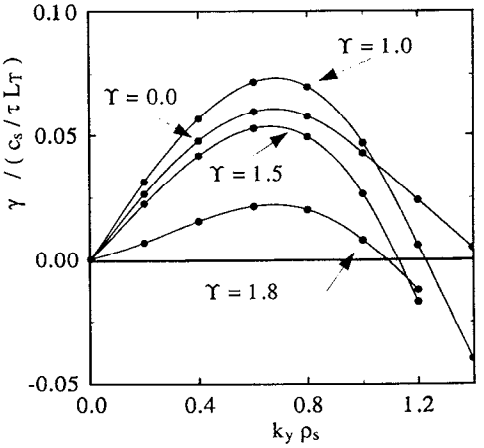

FIG. 5. The dispersion relation in the case of the flat density profile for different $\Upsilon = S_\perp/\sigma = L_s/L_V$. Here, $\sigma = 0.1$ and $\Gamma = 2$.

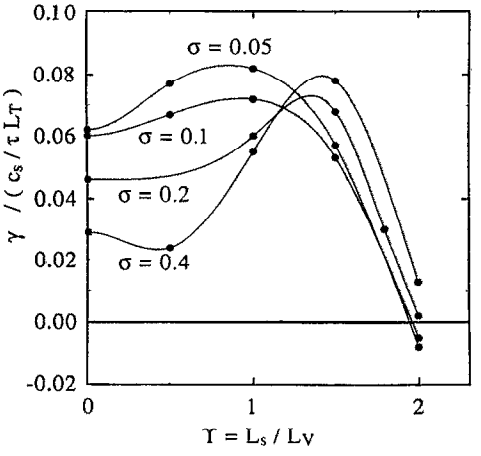

FIG. 6. The relation between the growth rate γ_G and the poloidal flow shear $\Upsilon = L_s/L_v$ for four different magnetic shear: $\sigma = 0.05$, 0.1, 0.2, and 0.4. Here, $k_y\rho_s = 0.6$ and $\Gamma = 2$.

magnetic shear values $\sigma = 0.05 - 0.4$, the critical value of Υ for stability is given by

$$\Upsilon_c \simeq 2,$$

in the case of a flat density profile.

IV. NONLINEAR NUMERICAL SIMULATIONS

We now solve the set of the nonlinear partial differential equations Eqs. (1)–(3) numerically in the 3-D domain and obtain the cross-field anomalous ion heat conductivity χ_i arising from the ITG-driven mode in the presence of finite sheared perpendicular (poloidal) flow. As in Sec. III, we do not consider sheared parallel (toroidal) flow ($S_\parallel = 0$). The anomalous ion heat conductivity χ_i is defined by

$$\chi_i = \frac{\overline{\langle \tilde{p}_i \tilde{v}_{ir} \rangle}}{-p_{i0}'} = -\frac{\rho_s}{L_n}\left(\frac{cT_e}{eB}\right)\overline{\left\langle p \frac{\partial \phi}{\partial y}\right\rangle} \ (K)^{-1}. \tag{36}$$

Here, the time average $\overline{g(t)}$ of a time-dependent function $g(t)$ is defined by

$$\overline{g(t)} = \lim_{T\to\infty} \frac{1}{T}\int_0^T g(t)dt$$

and the space average $\langle\ \rangle$, which is somewhat different from Eq. (4), is defined by

$$\langle\ \rangle = \frac{1}{\Delta L_y L_z}\int_{-L_x}^{L_x} d\tilde{x}\int_0^{L_y} d\tilde{y}\int_0^{L_z} d\tilde{z},$$

where Δ denotes the mode width in the x direction. In practice, the time average is taken over a reasonably long time period of T after the saturation is attained. The size of the mode width Δ is used as a normalization factor of Eq. (37) so that averaged values calculated from Eqs. (36) do not depend on choice of L_x when the modes are localized. In our simulations, the definition of Δ is given as follows; for a function $f(\tilde{x})$ representing a physical quantity averaged over $\tilde{y}$ and $\tilde{z}$, we define

$$I(\tilde{x}) = \begin{cases} 1, & \text{if } |f(\tilde{x})| \geqslant f_{\max}/10, \\ 0, & \text{if } |f(\tilde{x})| < f_{\max}/10, \end{cases}$$

where $f_{\max}$ is the maximum value of $|f(\tilde{x})|$ on $|\tilde{x}| \leqslant L_x$. Then the mode width Δ is defined by

$$\Delta = \int_{-L_x}^{L_x} I(\tilde{x})d\tilde{x},$$

which gives a reasonable estimate of the "support" of the localized mode. The fluctuation level of the space-averaged anomalous ion heat conductivity $\chi_i(t) = \langle p_i \tilde{v}_{ir}\rangle/(-p_{i0}')$ is then given by

$$\Delta\chi_i = \{\overline{[\chi_i(t) - \chi_i]^2}\}^{1/2}, \tag{37}$$

which is shown by error bars in the following figures for χ_i.

The initial value code used to solve Eqs. (1)–(3) is modified from the code used in Refs. 3 and 4. In the initial value code, Fourier representation for the $\tilde{y}$ and $\tilde{z}$ variables and a finite-difference scheme for the $\tilde{x}$ variable are employed. At each time step the dependent variables are advanced by means of the predictor–corrector method. The nonlinearity employed in the current version of the initial value code is due to the convective derivative $\{\phi,\ \}$ and the nonlinear finite-Larmor-radius terms

$$\{p, \Delta_\perp \phi\} + \left\{\frac{\partial p}{\partial \tilde{x}}, \frac{\partial \phi}{\partial \tilde{x}}\right\} + \left\{\frac{\partial p}{\partial \tilde{y}}, \frac{\partial \phi}{\partial \tilde{y}}\right\}$$

in Eq. (1). The boundary conditions are that all the physical variables be periodic in $\tilde{y}$ and $\tilde{z}$ with periods L_y and L_z, respectively, and they vanish at $|\tilde{x}| = L_x$, as discussed in Sec. II. We refer to the (m,n) mode of the Fourier representation as the mode whose $\tilde{y}$ and $\tilde{z}$ dependence is given by the phase $2\pi(m\tilde{y}/L_y - n\tilde{z}/L_z)$. The wave numbers $\tilde{k}_y$ and $\tilde{k}_z$ are thus given by $\tilde{k}_y = 2\pi m/L_y$ and $\tilde{k}_z = 2\pi n/L_z$. The rational surface of the (m,n) mode is located at $\tilde{x} = nL_y/msL_z$ since

$$\nabla_\parallel \propto \left(\frac{msx}{L_y} - \frac{n}{L_z}\right) = \left(\frac{ms}{L_y}\right)\left(x - \frac{nL_y}{msL_z}\right)$$

for the (m,n) mode. As initial conditions, small perturbations are given to each (m,n) mode at $\tilde{t} = 0$.

The size of the domain used throughout the following calculations is given by $L_x = 20$, $L_y = 10\pi$, and $L_z = 7.5\pi$, so that the smallest finite wave numbers are $k_y\rho_s = 0.2$ and $k_z L_n = 0.267$ and the distance between the two rational surfaces of the $m = 1/n = 0$ mode and the $m = 1/n = 1$ mode in the case of magnetic shear $s = 0.1$ is about $13\rho_s$. The equally spaced 150 mesh points are used for discretization of the interval $-L_x \leqslant \tilde{x} \leqslant L_x$ and 56 modes ($0 \leqslant m \leqslant 7$, $-3 \leqslant n \leqslant 3$) are chosen for the Fourier representation that cover at least all the unstable modes. The perpendicular diffusion parameters used in the simulations are $\mu_\perp = \chi_\perp = 0.1$. As noted in Sec. II, the parallel diffusion parameters $\mu_\parallel = \chi_\parallel = 1.0$ are chosen so as to model the collisionless ion Landau effect for high-temperature plasmas. In order to obtain turbulent saturation, rather than local quasilinear saturation, all the background quantities are kept constant (i.e., the $m = n = 0$ components of ϕ, v and p are set to be 0 at each time step).

Figure 7 shows the dependence of χ_i on the magnitude of the perpendicular sheared flow $\Upsilon = L_s/L_v$ for two differ-

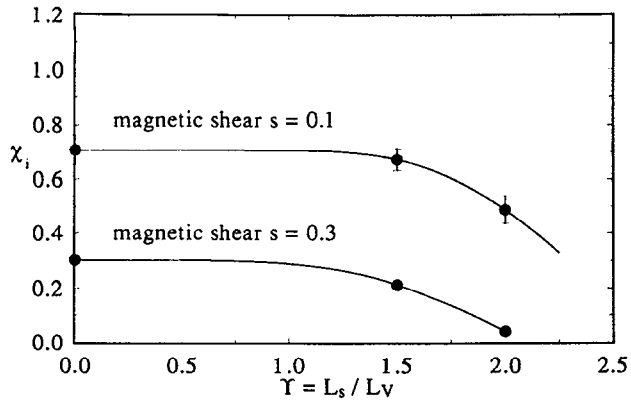

FIG. 7. The anomalous ion heat conductivity χ_i [normalized by $(\rho_s/L_n)(cT_e/eB)$] obtained from 3-D nonlinear simulations as a function of the poloidal flow shear $\Upsilon = L_s/L_V$ in two different magnetic shear $s = 0.1$ and 0.3. The parameters used here are $K = 3$, $\Gamma = 2$, $\mu_\perp = \chi_\perp = 0.1$, and $\mu_\parallel = \chi_\parallel = 1.0$.

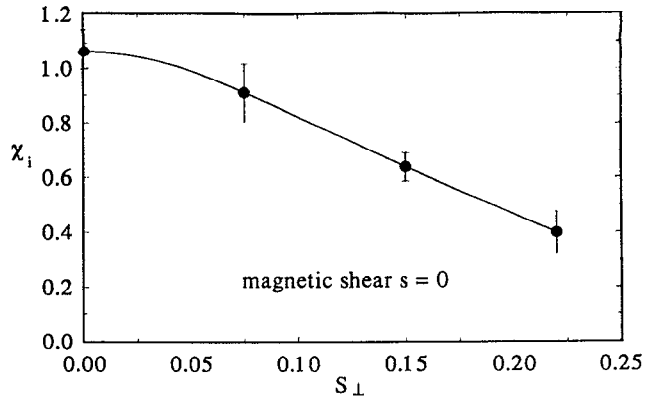

FIG. 9. The anomalous ion heat conductivity χ_i [normalized by $(\rho_s/L_n)(cT_e/eB)$] obtained from 3-D nonlinear simulations as a function of $S_\perp$ in zero magnetic shear ($s = 0$). The other parameters used in these calculations are the same as those of Fig. 6.

ent values of magnetic shear $s = 0.1$ and 0.3. As expected from linear properties of the mode discussed in Sec. II, χ_i is reduced significantly when $\Upsilon \gtrsim 2$. Figure 8 shows potential contours ($\phi = \text{const}$) at saturation in the case of $\Upsilon = 1.5$ and $s = 0.3$. The constant potential contours are the streamlines of the perturbed $\mathbf{E}\times\mathbf{B}$ flow: The streamlines of the mean flow are not shown in Fig. 8. It is seen that the vortex cells are considerably elongated in the y direction due to the sheared flow. There are seven rational surfaces for the $m = 1$ modes, located at $x/\rho_s = 0, \pm 4.4, \pm 8.9$, and ± 13.3 (and more rational surfaces for higher m modes) in the domain of Fig. 8. Figure 9 shows the χ_i dependence on the sheared perpendicular flow $S_\perp$ in the case of zero magnetic shear ($s = 0$), in which $\Upsilon = S_\perp/s = \infty$. It is observed that $S_\perp$, rather than $\Upsilon = L_s/L_V$, becomes a characteristic parameter in determining χ_i when the magnetic shear $s \lesssim 0.1$. From Figs. 7 and 9, the anomalous ion heat conductivity χ_i in weak magnetic shear ($s \lesssim 0.1$) is shown to be reduced significantly when $S_\perp \gtrsim 0.2$. The other parameters chosen for Figs. 7–9 are $K = T_i(1+\eta_i)/T_e = 3$ and $\Gamma = 2$.

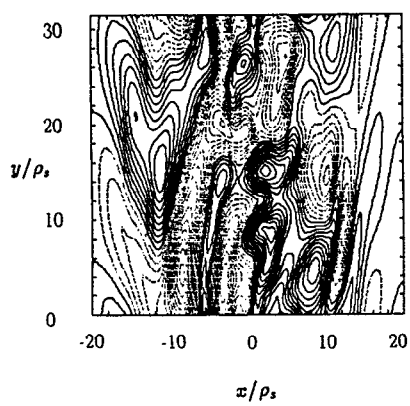

FIG. 8. Potential contours ($\phi = \text{const}$) at a nonlinearly saturated state when $\Upsilon = 1.5$ and $s = 0.3$. The other parameters are the same as those of Fig. 7.

V. DISCUSSION AND CONCLUSIONS

We have shown based on linear and nonlinear calculations that the ITG-driven turbulence is significantly reduced in the presence of sufficiently strong sheared poloidal flows as characterized by the parameter $\Upsilon = L_s/L_V \simeq \Upsilon_c$, where

$$\Upsilon_c \simeq 2\sqrt{(1+\eta_i)T_i/T_e}$$

denotes the critical value of Υ. The condition of such reduction of the ITG turbulence is, therefore, also given by

$$\frac{dv_E}{dx} \simeq \frac{2c_s}{L_s}\sqrt{\frac{(1+\eta_i)T_i}{T_e}}\,.$$

The linear calculations show that this reduction of the ITG mode activity is basically attributed to linear stabilization due to the sheared poloidal flows, rather than a nonlinear stabilization. It is also shown analytically and numerically that weak sheared flows ($\Upsilon \ll 1$) increases the linear growth rate of the ITG mode as Υ^2 [see Eq. (25)], whereas the aforementioned reduction of the growth rate and stabilization occur when $\Upsilon = \mathcal{O}(1)$. Three-dimensional nonlinear calculations demonstrate that the ITG-driven turbulence and the associated anomalous ion heat transport coefficient χ_i are reduced significantly when $\Upsilon \simeq \Upsilon_c$ in a realistic parameter range of $K = (1+\eta_i)T_i/T_e$ and $s = L_n/L_s$.

These conditions are well satisfied in the shear-flow boundary layer of tokamaks. For example, in TEXT the sheared poloidal flow (the $\mathbf{E}\times\mathbf{B}$ flow v_E) has been found to be greater than $dv_E/dx\,(= V_0') \simeq 10^5$ sec^{-1} in the edge boundary layer where $L_s \geqslant 200$ cm giving $L_s\, dv_E/dx \simeq 2\times 10^7$ cm/sec which would exceed c_s unless the edge temperature $T_e > 500$ eV. At the actual temperature in the shear layer $T_e \simeq 50$ eV the parameter Υ is several times greater than Υ_c and the experiment shows a local reduction in the fluctuation level of $\tilde{\phi}$ as shown in Fig. 1 of Ritz *et al.*[11]

In the DIII-D tokamak (Groebner *et al.*[14]) the onset of the high-confinement regime (H mode) appears to follow the increase of the sheared poloidal flow inferred from Doppler shift measurements of spectral lines inside and out-

side the shear flow layer of width $L_E = |v_E/(dv_E/dx)| = 2 \sim 3$ cm. In this case the value of the perpendicular flow v_E is reported to increase from 5 to 15 km/sec in the time (5–10 msec) required to go from the low- to high-confinement regime. For $L_s = 300$ cm and $c_s = 3 \times 10^7$ cm/sec (values not given in Groebner *et al.*[14]) the dimensionless parameter Υ would increase from 1.7 to 5 in this transition. Certainly, such a change in Υ would predict a dramatic reduction in the ion thermal diffusivity $\chi_i(K,\Upsilon)$ from our theory and simulations.

ACKNOWLEDGMENT

This research was supported by U.S. Department of Energy Contract No. DE-FG05-80ET-53088.

APPENDIX: INTEGRAL FORMULAS

Here we summarize the integral formulas used in Sec. III. Writing $u_l(\xi) = e^{-\xi^2/2} H_l(\xi)$ with Hermitian function $H_l(\xi) = (-1)^l e^{\xi^2} (d^n e^{-\xi^2}/d\xi^n)$, we have

$$\langle u_n u_m \rangle = \begin{cases} 2^n n! \sqrt{\pi} & (n = m), \\ 0 & (n \neq m), \end{cases}$$

$$\langle \xi u_n u_m \rangle = \begin{cases} 2^{n-1} n! \sqrt{\pi} & (n = m+1), \\ 2^n (n+1)! \sqrt{\pi} & (n = m-1), \\ 0 & (\text{otherwise}), \end{cases}$$

$$\langle \xi^2 u_n u_m \rangle = \begin{cases} 2^{n-2} n! \sqrt{\pi} & (n = m+2), \\ 2^{n-1} (2n+1) n! \sqrt{\pi} & (n = m), \\ 2^n (n+2)! \sqrt{\pi} & (n = m-2), \\ 0 & (\text{otherwise}), \end{cases}$$

$$\langle \xi^3 u_n u_m \rangle = \begin{cases} 2^{n-3} n! \sqrt{\pi} & (n = m+3), \\ 3 \cdot 2^{n-2} n n! \sqrt{\pi} & (n = m+1), \\ 3 \cdot 2^{n-1} (n+1)(n+1)! \sqrt{\pi} & (n = m-1), \\ 2^n (n+3)! \sqrt{\pi} & (n = m-3), \\ 0 & (\text{otherwise}), \end{cases}$$

$$\langle \xi^4 u_n u_m \rangle = \begin{cases} 2^{n-4} n! \sqrt{\pi} & (n = m+4), \\ 2^{n-2} (2n-1) n! \sqrt{\pi} & (n = m+2), \\ 3 \cdot 2^{n-2} (2n^2 + 2n + 1) n! \sqrt{\pi} & (n = m), \\ 2^n (2n+3)(n+2)! \sqrt{\pi} & (n = m-2), \\ 2^n (n+3)! \sqrt{\pi} & (n = m-4), \\ 0 & (\text{otherwise}), \end{cases}$$

$$\langle u_n u_m' \rangle = \begin{cases} -2^{n-1} n! \sqrt{\pi} & (n = m+1), \\ 2^n (n+1)! \sqrt{\pi} & (n = m-1), \\ 0 & (\text{otherwise}), \end{cases}$$

$$\langle \xi u_n u_m' \rangle = \begin{cases} -2^{n-2} n! \sqrt{\pi} & (n = m+2), \\ -2^{n-1} n! \sqrt{\pi} & (n = m), \\ 2^n (n+2)! \sqrt{\pi} & (n = m-2), \\ 0 & (\text{otherwise}). \end{cases}$$

Here, the prime denotes $d/d\xi$.

[1] R. E. Waltz, Phys. Fluids **31**, 1962 (1988).
[2] F. Romanelli, Phys. Fluids B **1**, 1018 (1989).
[3] S. Hamaguchi and W. Horton, Phys. Fluids B **2**, 1833 (1990).
[4] S. Hamaguchi and W. Horton, Phys. Fluids B **2**, 3040 (1990).
[5] J. Liu, W. Horton, and J. E. Sedlak, Phys. Fluids **30**, 467 (1987); W. Horton and J. Liu, *ibid.* **27**, 2067 (1984).
[6] W. Horton, T. Tajima, and T. Kamimura, Phys. Fluids **30**, 3485 (1987).
[7] K. C. Shaing, E. C. Crume, and W. A. Houlberg, Phys. Fluids B **2**, Part 2, 1492 (1990).
[8] T. Tajima, W. Horton, P. J. Morrison, J. Schutkeker, T. Kamimura, and K. Mima, Phys. Fluids B **3**, 938 (1991).
[9] Theilhaber and C. K. Birdsall, Phys. Rev. Lett. **62**, 772 (1989); Phys. Fluids B **1**, 2244 (1989).
[10] Ch. P. Ritz, R. D. Bengtson, and S. J. Levinson, Phys. Fluids **27**, 2956 (1984).
[11] Ch. P. Ritz, H. Lin, T. L. Rhodes, and A. J. Wootton, Phys. Rev. Lett. **65**, 2543 (1990).
[12] R. J. Taylor, M. J. Brown, B. D. Fried, H. Grote, J. R. Liberati, G. J. Morales, P. Pribyl, D. Darrow, and M. Ono, Phys. Rev. Lett. **63**, 2365 (1989).
[13] K. H. Burrell, T. N. Carlstrom, E. J. Doyle, P. Gohil, R. J. Groebner, T. Lehecka, N. C. Luhmann, Jr., H. Matsumoto, T. H. Osborne, W. A. Peebles, and R. Philipona, Phys. Fluids B **2**, Part 2, 1405 (1990).
[14] R. J. Groebner, K. H. Burrell, and R. P. Seraydarian, Phys. Rev. Lett. **64**, 3015 (1990).
[15] S. Hamaguchi and W. Horton, to appear in Plasma Phys. Controlled Fusion.
[16] M. Kotschenreuther, H. L. Berk, R. Denton, S. Hamaguchi, W. Horton, C.-B. Kim, M. Lebrun, P. Lyster, S. Mahajan, W. H. Miner, P. J. Morrison, D. Ross, T. Tajima, J. B. Taylor, P. M. Valanju, H. V. Wong, S. Y. Xiao, and Y.-Z. Zhang, *Plasma Physics and Controlled Nuclear Fusion Research*, Proceedings of the 13th International Conference, Washington DC, 1990 (IAEA, Vienna, 1991), Vol. II, p. 361.
[17] G. Hammett and F. Perkins, Phys. Rev. Lett. **64**, 3019 (1990).
[18] S. I. Braginskii, in *Review of Plasma Physics*, edited by M. A. Leontovich (Consultants Bureau, New York, 1965), Vol. 1, p. 205.
[19] W. Horton, D. I. Choi, and W. M. Tang, Phys. Fluids **24**, 1077 (1981).
[20] J. Y. Kim and W. Horton, Phys. Fluids B **3**, 1167 (1991).
[21] R. S. B. Ong and N. Roderick, Planet. Space Sci. **20**, 1 (1972).
[22] Similar behavior is observed for an ideal MHD mode in sheared equilibrium flows. See A. Bonderson, R. Iacono, and A. Bhattacharjee, Phys. Fluids **30**, 2167 (1987).